ARTICLE
Journal of Cellular Biochemistry 114:929–941 (2013)

Journal of Cellular Biochemistry

Luteolin Inhibition of V-ATPase *a3–d2* Interaction Decreases Osteoclast Resorptive Activity

Gazelle J. Crasto,[1] Norbert Kartner,[1] Yeqi Yao,[1] Keying Li,[1] Liv Bullock,[1] Alessandro Datti,[2,3] and Morris F. Manolson[1,4*]

[1] *Faculty of Dentistry, Dental Research Institute, University of Toronto, Toronto, Ontario, Canada M5G 1G6*
[2] *Samuel Lunenfeld Research Institute, Mt. Sinai Hospital, Toronto, Ontario, Canada M5G 1X5*
[3] *Department of Experimental Medicine and Biochemical Sciences, University of Perugia, Perugia 06100, Italy*
[4] *Faculty of Medicine, Department of Biochemistry, University of Toronto, Toronto, Ontario, Canada M5S 1A8*

ABSTRACT

V-ATPase-mediated acid secretion is required for osteoclast bone resorption. Osteoclasts are enriched in V-ATPase *a3* and *d2* subunit isoforms, and disruption of either of their genes impairs bone resorption. Using purified fusion proteins of *a3* N-terminal domain (NT*a3*) and full-length *d* subunits we determined in a solid-phase binding assay that half-maximal binding of *d1* or *d2* to immobilized NT*a3* occurs at 3.1 ± 0.4 or 3.6 ± 0.6 nM, respectively, suggesting equally high-affinity interactions. A high-throughput modification of this assay was then used to screen chemical libraries for *a3–d2* interaction inhibitors, and luteolin, a naturally occurring flavonoid, was identified, with half-maximal inhibition at 2.4 ± 0.9 μM. Luteolin did not significantly affect NIH/3T3 or RAW 264.7 cell viability, nor did it affect cytokine-induced osteoclastogenesis of RAW 264.7 cells or bone marrow mononuclear cells at concentrations $\leq$40 μM. Luteolin inhibited osteoclast bone resorption with an EC_{50} of approximately 2.5 μM, without affecting osteoclast actin ring formation. Luteolin-treated osteoclasts produced deeper resorption pits, but with decreased surface area, resulting in overall decreased pit volume. Luteolin did not affect transcription, or protein levels, of V-ATPase subunits *a3*, *d2*, and E, or V_1V_0 assembly. Previous work has shown that luteolin can be effective in reducing bone resorption, and our studies suggest that this effect of luteolin may be through disruption of osteoclast V-ATPase *a3–d2* interaction. We conclude that the V-ATPase *a3–d2* interaction is a viable target for novel anti-resorptive therapeutics that potentially preserve osteoclast–osteoblast signaling important for bone remodeling. J. Cell. Biochem. 114: 929–941, 2013.

KEY WORDS: VACUOLAR H^+-ATPase; PROTON TRANSPORT; BIOFLAVONOIDS; OSTEOPOROSIS; DRUG DISCOVERY

Osteoclasts are multinucleate bone-resorbing cells essential for plasma calcium homeostasis and bone remodeling, thereby maintaining the structural and mechanical integrity of bone [Henriksen et al., 2011]. Bone resorption is achieved, in part, by the recruitment of V-ATPases to the plasma membranes of polarized, active osteoclasts, where they mediate extracellular acidification [Hinton et al., 2009a]. In post-menopausal women, estrogen deficiency leads to an imbalance in remodeling, with increased osteoclast resorptive activity resulting in pathological bone loss. Thus, factors that control osteoclast resorptive activity, including V-ATPase-mediated acid secretion, are potential targets for the development of anti-resorptive therapeutics.

Mammalian V-ATPases are complexes assembled from 14 different subunits that are organized within two functional sectors [Zhang et al., 2008b]. The peripheral V_1 sector, located in the cytoplasm, is composed of subunits A–H, and its A_3B_3 catalytic headpiece hydrolyzes ATP providing the driving force for the proton pump. The integral membrane V_0 sector consists of *a*, *c*, *c″*, *d*, *e*, and *Ac45* subunits and is involved in transmembrane proton translocation. V-ATPase activity is regulated, in part, by the dissociation/reassociation of its V_1 and V_0 sectors [Toei et al., 2010]. The *a* subunit is the largest (ca. 100 kDa), with a hydrophobic carboxyl (C)-terminal domain (CT*a*; ca. 50 kDa) within the V_0 sector and a hydrophilic amino (N)-terminal domain (NT*a*; ca. 50 kDa) that interacts with the V_1 sector [Kartner et al., 2010].

The authors declare no conflicts of interest.

Grant sponsor: Canadian Institutes of Health Research; Grant number: FRN79322; Grant sponsor: Canadian Arthritis Network; Grant number: 2008-02-DAP-02.

*Correspondence to: Morris F. Manolson, Faculty of Dentistry, University of Toronto, 124 Edward St., Toronto, Ontario, Canada M5G 1G6. E-mail: m.manolson@dentistry.utoronto.ca

Manuscript Received: 29 June 2012; Manuscript Accepted: 22 October 2012

Accepted manuscript online in Wiley Online Library (wileyonlinelibrary.com): 5 November 2012

DOI 10.1002/jcb.24434 • © 2012 Wiley Periodicals, Inc.

Some mammalian V-ATPase subunits have multiple isoforms, for example, *a1–4*, *d1*, and *d2*. It is thought that V-ATPases with different *a* subunit isoforms are targeted to different membranes [Manolson et al., 1994; Kawasaki-Nishi et al., 2001; Finnigan et al., 2011]. We have found that the *a3* subunit isoform is highly expressed in osteoclasts, with over 100-fold greater expression than in liver, the tissue with the next highest expression level [Manolson et al., 2003]. The *a3* subunit isoform is induced during osteoclast differentiation and traffics to the plasma membrane as part of the V-ATPase complex that is specific for osteoclast acid secretion [Toyomura et al., 2000]. Ablation of the mouse *a3* genes, and naturally occurring human mutations, result in osteopetrosis, a sclerosing bone disease resulting from inadequate bone resorption [Sobacchi et al., 2001; Scimeca et al., 2003; Pangrazio et al., 2012]. In mammals, the *d2* isoform is also most highly expressed in the ruffled borders of resorbing osteoclasts [Lee et al., 2006]. No *d2* mutations have been reported to date, but *d2* ablation in mice also yields an osteopetrosis phenotype. Furthermore, the mouse *d2* knockout model shows reduction of osteoclast function and increased osteoblast bone deposition [Lee et al., 2006]. Thus, targeting *d2* may have both anti-resorptive and anabolic therapeutic potential.

General V-ATPase inhibitors reduce bone resorption [Niikura, 2007], but they are cytotoxic, as V-ATPases are essential for a variety of vital intracellular functions. Targeting function-specific V-ATPases may be possible, as it is hypothesized that specialized V-ATPases may have unique combinations of subunit isoforms. For example, the combination of *a3*, *d2*, and *B2* subunit isoforms is thought to be a signature feature of acid-secreting V-ATPases in the osteoclast plasma membrane. In previous work, we identified a small-molecule benzohydrazide derivative that inhibits the *a3*–B2 subunit interaction, and this compound was found to reduce bone resorption in vitro [Kartner et al., 2010]. The *a3* and *d2* subunits are also known to interact [Wu et al., 2009; Kim et al., 2010], and it seems possible that a similar strategy could be employed to find inhibitors of the *a3–d2* interaction. Thus, in the present work we characterized *a3–d1* and *a3–d2* interactions, using purified fusion proteins, and implemented a high-throughput ELISA screen to identify compounds that inhibit the interaction. A primary hit identified in this screen was the flavonoid, luteolin.

Flavonoids are bioactive phenols that have been shown to have anti-oxidant, anti-inflammatory, anti-allergic, anti-microbial, and anti-cancer activity [Kandaswami et al., 2005; Seelinger et al., 2008]. Luteolin belongs to the flavone class of flavonoids commonly found in fruits, vegetables, and medicinal herbs. Here we show that luteolin prevents V-ATPase *a3–d2* protein–protein interaction and that it inhibits V-ATPase-mediated acid secretion at micromolar concentrations, decreasing osteoclast bone resorption without affecting osteoclast differentiation or viability.

MATERIALS AND METHODS

REAGENTS AND ANTIBODIES

Phosphate buffered saline (PBS) was 0.2 g/L KCl, 0.2 g/L KH_2PO_4, 8.0 g/L NaCl, 1.15 g/L Na_2HPO_4, pH 7.4. PBST was PBS with 0.05% Triton X-100 (Sigma). Tris buffered saline with Triton X-100 (TBST) was 20 mM Tris–HCl, 0.9% (w/v) NaCl, 0.05% (w/v) Triton X-100, pH 7.40. All buffer pH values were adjusted at 25°C. Luteolin (Sigma L9283) was dissolved in distilled water with addition of a small amount of 1 N NaOH to effect dissolution of the powder. The 5 mM stock solution was stored at −20°C. Gelatin used as a blocking agent in pulldown assays and ELISA was EIA grade (Bio-Rad). Glutathione sepharose 4B was from GE Healthcare and Ni-NTA agarose was from Qiagen. Anti-GST antibody was rabbit polyclonal GST(Z-5) from Santa Cruz Biotechnology (catalog no. sc-459). Anti-His-tag antibody was mouse monoclonal His-Probe (H-3) from Santa Cruz (sc-8036); horseradish peroxidase (HRP)-conjugated goat anti-mouse IgG (HRP-GAM) was from Santa Cruz (sc-2005). Rabbit anti-β-actin monoclonal antibody (13E5) was from cell signals technology (4970); HRP-conjugated polyclonal goat anti-rabbit IgG (HRP-GAR) was from Santa Cruz (sc-2004). V-ATPase subunit antibodies, anti-*a3* and anti-E were gifts from Dr. Beth S. Lee (Ohio State University, Columbus, OH), and anti-*d2* antibody was a gift from Alethia Biotherapeutics (Montreal, Canada).

CELL CULTURE

Murine macrophage RAW 264.7 cells (ATCC accession no. TIB-71) were cultured in high-glucose DMEM (Invitrogen 11995) supplemented with 10% (v/v) FBS (Invitrogen 10437-028), 100 units/ml penicillin and 100 μg/ml streptomycin. RAW 264.7 cells were differentiated into osteoclasts in α-MEM (Invitrogen 12561) supplemented with 10% (v/v) FBS, 100 units/ml penicillin, 100 μg/ml streptomycin, and 100 ng/ml soluble recombinant RANKL for 5 days with change of medium on Day 3. Bone marrow mononuclear (BMM) cells were isolated from tibias and femurs of 6-week-old CD-1 mice. The cells were seeded in 96-well microtiter plates at 1×10^5 cells/well in α-MEM supplemented with 15% (v/v) FBS, 100 units/ml penicillin, 100 μg/ml streptomycin, and 50 ng/ml M-CSF (EMD-Calbiochem 234378) and grown for 2 days. Cells were differentiated into osteoclasts in the presence of 100 ng/ml soluble recombinant RANKL and 50 ng/ml M-CSF for an additional 5 days. Cell culture was at 37°C in a humidified 5% CO_2 incubator.

CONSTRUCTS

The plasmid construct expressing the N-terminal thioredoxin (TRX, with His-tag) fusion of the N-terminal domain of the mouse V-ATPase *a3* subunit, TRX-NT*a3*, was constructed as previously described [Kartner et al., 2010]. Constructs expressing N-terminal glutathione-S-transferase (GST) fusions with full-length mouse V-ATPase *d1* and *d2* subunits, GST-*d1* and GST-*d2*, were prepared using reverse-transcription PCR strategies described previously [Kartner et al., 2010], from mouse brain and mouse kidney mRNA, with the oligonucleotide primers listed in Table I.

PURIFICATION OF FUSION PROTEINS

Fusion proteins were purified by glutathione or nickel (II) affinity chromatography, essentially as described by Kartner et al. [2010]. For GST-*d1* and GST-*d2* fusion proteins, exponentially growing bacteria expressing the proteins were induced with 0.2 mM IPTG and incubated for 16 h at 16°C. Cells were harvested and resuspended in PBS containing 0.2 mg/ml lysozyme per 200 ml of original culture volume, incubated on ice for 30 min and mixed with 2.5 volumes of

TABLE I. Primers, Plasmid Constructs, and Protein Expression Products

Subunit (domain)[a] [Template, PCR primers (sense/anti-sense)]	Expression plasmid[b]	Product (a.a.)[c]
a3 (NT*a3* domain) [pcDNA 3.1-*a3*, 5′-gaattcggtggtatgggctctatgttccggagtgaagag-3′ 5′-gtcgacattaggtgtagggagcagggttaacttccc-3′]	pET32a-NT*a3*	TRX(H6)-G_2-NT*a3*$^{(1-393)}$
d1 (full-length) [mouse brain cDNA, 5′-gaattcggaggtatgtcgttctt-3′ 5′-gtcgactaaaagatggggatgtagttgtc-3′]	pGEX-4T1-*d1*	GST-G_2-*d1*$^{(1-351)}$
d2 (full-length) [mouse kidney cDNA, 5′-gaattcggtggtatgcttgagactgcagagctgtacttcaatgtgg-3′ 5′-gtcgactattataaaattggaatgtagctgttgattttagttcgatgcc-3′]	pGEX-4T1-*d2*	GST-G_2-*d2*$^{(1-350)}$

[a]The *a3* subunit was cloned partially, as its hydrophilic amino-terminal (NT) cytoplasmic domain; *d* subunits were full length; all V-ATPase subunits were of mouse origin; all PCR primers had a short, random 5′ extension (not shown) to improve restriction enzyme cleavage.
[b]pET constructs were in pET32a(+), pGEX constructs in pGEX-4T-1; PCR products were *Eco*RI/*Sal*I digested and ligated into *Eco*RI/*Sal*I digested vectors; all constructs were verified by full-length sequencing of inserts and junctions.
[c]Expressed protein domain organization is indicated—TRX(H_6) and GST are N-terminal *E. coli* thioredoxin (with His-tag and S-tag domains) and *S. japonicum* glutathione-S-transferase fusions, respectively; G_2 is a Gly–Gly coupler; in superscript parentheses are shown the amino acid ranges (a.a.) of the expressed subunits (homologous target V-ATPase subunit sequence only, numbered with respect to the natural subunit N-terminal methionine).

ice-cold 0.2% (w/v) Triton X-100 and sonicated. DNase I (5 μg/ml) and RNase A (10 μg/ml) were added and the mixture was incubated on ice for an additional 10 min. After centrifugation at 20,000*g* for 15 min, the supernatant was withdrawn and mixed, at 10 ml/L of starting culture, with a 50% slurry of glutathione-sepharose 4B in PBS and allowed to incubate for 1 h at 4°C with rocking. Beads were collected by centrifugation at 500*g* for 5 min and were transferred to a Poly-Prep chromatography column (Bio-Rad) and eluted with 10 mM glutathione in 50 mM Tris–HCl. Fractions were collected and analyzed by SDS–PAGE.

IMMUNOBLOT ANALYSIS

Primary and secondary antibodies were as described. Images were developed with Western Lightning ECL detection solution (PerkinElmer) and blots were imaged in a Bio-Rad Molecular Imager ChemiDoc XRS system and quantified using Quantity One 4.6.9 software.

PULLDOWN ASSAYS

Affinity pulldown assays were done by first coating 150 μl of a 50% suspension of beads (glutathione beads for GST-*d1*, GST-*d2*, and unfused GST control; Ni(II) beads for TRX-NT*a3*) in 600 μl of PBST containing 2 mM ditihiothreitol (DTT) and 40 μg of the ligand fusion protein for 1 h at 8°C, with rocking. After several washes with PBST at 4°C, 40 μg of analyte protein was added in 600 μl PBST containing 2 mM DTT and a further 1 h incubation was done at 8°C, with rocking. Beads were then washed five times with 1 ml ice-cold PBST and pelleted beads were eluted with 100 μl of SDS sample buffer and 10 μl samples were run on SDS–PAGE and immunoblotted with a 1:2,500 dilution of either anti-His-tag antibody, or anti-GST antibody, followed by secondary antibodies, HRP-GAM, or HRP-GAR, respectively.

IN VITRO ELISA-BASED SOLID-PHASE BINDING ASSAYS

Methods for obtaining protein–protein saturation binding curves were essentially as previously reported by Kartner et al. [2010]. Briefly, high protein-binding polystyrene 384-well plates (Greiner Microlon 781097) were coated with ligand protein (10 μg/ml TRX-NT*a3*) in protein coating buffer (10 mM sodium phosphate, pH 7.0) overnight at 4°C. Coated plates were washed twice with TBST, blocked for 1 h with blocking buffer [1% (w/v) gelatin and 0.1% (w/v) phenol in TBST, pH 7.40] and washed twice again with TBST. Wells were then incubated with analyte protein, GST-*d1*, or GST-*d2*, in blocking buffer for 1 h, followed by three consecutive washes. Anti-GST antibody in blocking buffer was added to the wells and incubated for 30 min. Plates were washed again and incubated with secondary HRP-GAR antibody in blocking buffer for 30 min. Plates were then washed and freshly prepared developer solution was added (80 μg/ml; 3,3′,5,5′-tetramethylbenzidine, 0.01% hydrogen peroxide, 0.1 M sodium acetate, pH 6.0). After 15 min the reaction was stopped with 1 N sulfuric acid and absorbance was quantified using a PerkinElmer Envision Multilabel Reader at 450 nm, with subtraction of an optical reference absorbance at 600 nm.

HIGH-THROUGHPUT CHEMICAL LIBRARY SCREENING

This assay was developed to identify compounds that inhibit the V-ATPase *a3–d2* subunit interaction and was executed essentially as described by Kartner et al. [2010], except that the analyte protein was the GST-*d2* fusion protein instead of GST-B2. Briefly, the same protocol was carried out as outlined in the ELISA-based solid-phase binding assay, above, except each well was pre-incubated with a compound from a chemical library before the GST-*d2* analyte protein was added. The high-throughput assays were carried out at the Samuel Lunenfeld Research Institute SMART robotics facility (Mt. Sinai Hospital, Toronto, Canada), as described [Kartner et al., 2010]. Hits were assigned a score after data analysis was carried out using B score statistics and were ranked according to negative deviation from the mean B score. Selected hits, falling at least 3 SD below the mean, were confirmed by repeating the primary assay screen. Hits that were reproducible were tested for dose response in the protein-binding assay and in secondary cellular screening assays for toxicity. Only one primary hit, the natural product, luteolin, passed these criteria and was deemed suitable for further study.

CELL TOXICITY ASSAYS

To evaluate the effect of primary hits on metabolic activity, a modified mitochondrial reductase activity assay based on tetrazolium dye (MTS) reduction was used. Cells were seeded in 96-well

tissue culture plates at 5×10^3 cells/well in 150 μl of medium per well and allowed to grow for 2 days in the presence or absence of the test compound. For quantification, 20 μl of reagent (CellTiter 96 Aqueous One Solution Cell Proliferation Assay solution; Promega G3582) was added to individual wells and absorbances were read at 490 nm after overnight incubation with the dye.

Protein assays were used to determine cell growth in the presence and absence of test compounds. Initially, 5×10^3 cells in 200 μl volumes were seeded in 96-well plates and the cells were allowed to grow for 3 days in the presence and absence of test compounds. Cells were washed with PBS and lysed with protein lysis buffer (90 mM trisodium citrate, 10 mM NaCl, 0.1% Triton X-100, pH 4.8). Protein concentration was determined using the Pierce 660 nm protein assay (Thermo Scientific 22662).

TARTRATE-RESISTANT ACID PHOSPHATASE (TRAP) ASSAY

Two methods were used, one a histological TRAP stain for fixed cells and the other an assay for total soluble TRAP activity from cells permeabilized with an acidic detergent buffer. Fixed cells were TRAP stained according to the BD BioSciences TRAP staining protocol no. 445. For total soluble TRAP assays, cells were differentiated into osteoclasts for 5 days in 96-well tissue culture plates, medium was aspirated on Day 5, and cells were washed twice with PBS and lysed for TRAP determination. Protocols for both methods were as previously described [Kartner et al., 2010].

HYDROXYLAPATITE RESORPTION ASSAY

Resorption assays on the Corning Osteo Assay surface (Corning Lifesciences) were performed as described [Kartner et al., 2010]. Briefly, RAW 264.7, or BMM cells, were differentiated into osteoclasts on Corning Osteo Assay surface 96-well plates. Cells were allowed to attach to plates for 2 h at 37°C, and then 100 μl of medium containing 100 ng/ml RANKL and varying concentrations of luteolin was added to each well. A complete change of medium was carried out on Day 3. On Day 5, cells were stripped from plates with 150 μl of 1.2% sodium hypochlorite for 5 min. The plates were then aspirated, washed thoroughly with water and air dried prior to staining. Modified von Kossa staining was used to increase the contrast of the Osteo Assay surface, as described [Kartner et al., 2010].

IVORY RESORPTION ASSAY

An Isomet slow speed saw with a 4 in. diameter diamond wafering blade was used to cut 100–150 μm thick ivory slices that were then 0.25 in. hole-punched to fit into wells of a 96-well plate. Ivory discs were stored in 20% (v/v) ethanol. For resorption assays, discs were washed with 70% (v/v) ethanol, followed by sterile PBS and incubated overnight in medium at 37°C in a tissue culture incubator. BMM cells were isolated and differentiated into osteoclasts as described above, but after 4 days of differentiation osteoclasts were dissociated using cell dissociation buffer (Gibco 13151-014) and were replated onto ivory in the presence of varied concentrations of luteolin and incubated until Day 9 or 10. Prior to microscopic observation, ivory discs were washed twice with 70% (v/v) ethanol and twice with cold PBS, sonicated in PBS, and washed several times in PBS to remove cell debris.

PICRO-SIRIUS RED STAINING OF IVORY SLICES TO VISUALIZE RESORPTION PITS

Resorbed ivory slices were washed in distilled water three times and immersed in 0.1 M phosphate buffer, pH 7.4, then incubated in 12 units/ml of papain (Sigma 76218) for 90 min at 37°C, followed by Picro-Sirius Red stain (Sigma 43665) for 60 min at room temperature. After staining, slices were washed twice with 0.1 M HCl for 2 min and dehydrated in 70%, 90%, and 100% graded ethanol baths, followed by immersion in 70%, 90%, and 100% graded xylene baths. Entellan new rapid mounting medium (EMD 65037-71) was used to mount slices on glass slides, which were stored at 4°C. A Zeiss 100M LSM 510 confocal microscope was used to evaluate pit depth and pit area on ivory slices. Three independent experiments were performed in which 15 fields were measured for pit depth and pit area for each group. ImageJ (NIH) and Volocity (PerkinElmer) software were used to quantify total pit depth and total pit area.

PHALLOIDIN STAINING

Briefly, BMM-differentiated osteoclasts were cultured on ivory slices, the cells were then rinsed with PBS and fixed and permeabilized as described by McMichael et al. [2006]. Rhodamine-conjugated phalloidin was used to stain F-actin and cell staining was visualized by confocal microscopy.

OSTEOCLAST MEMBRANE PREPARATIONS

Microsomal membranes from RAW 264.7 cell-derived osteoclasts were prepared according to the modified method of Baron et al. [David and Baron, 1994]. Briefly, RAW 264.7 cells were differentiated into osteoclasts in the presence and absence of luteolin for 5 days. Cells were washed with homogenization buffer (230 mM sucrose, 40 mM KCl, 20 mM HEPES–KOH, 2 mM DTT, pH 7.0) and homogenized using 50 strokes in a Dounce homogenizer. Homogenate was centrifuged for 10 min at 4,000*g* at 4°C to pellet unbroken cells, nuclei, and mitochondria. Supernatants were collected on ice and centrifuged at 100,000*g* for 40 min and the pellet was resuspended in ice-cold buffer consisting of 150 mM KCl, 20 mM HEPES–KOH, 2 mM DTT, pH 7.4. Membranes were stored at −20°C and used subsequently for assays of ATP hydrolysis and immunoblotting.

STATISTICS

Repetition of experiments is noted in figure legends. Determination of IC_{50} or EC_{50} values for dose-response curves, or half-maximal binding in protein interaction assays, was done using GraphPad Prism 4 curve-fitting software. Standard deviations were calculated and are shown as ±1 SD wherever values are quoted, or in error bars in histograms and graphs. Unpaired two-tailed *t*-tests were used to test significance of differences, as appropriate.

RESULTS

INTERACTION OF V-ATPase *a3* AND *d2* SUBUNIT ISOFORMS

Affinity pulldown assays using recombinant fusion proteins demonstrated that the N-terminal domain of the V-ATPase *a3* subunit (NT*a3*) could pull down the *d2* subunit from solution

(Fig. 1A). This qualitatively demonstrated an interaction between *a3* and *d2*, but to quantitatively compare apparent binding affinities of *a3–d* interactions we used an ELISA-based solid-phase binding assay, as previously described for NT*a3*–B interactions [Kartner et al., 2010]. V-ATPase *d1* and *d2* subunits (analyte proteins, as GST fusions) were tested against bound NT*a3* (ligand, fused with TRX), as shown in Figure 1B. The half-maximal binding values calculated from saturation curves for NT*a3–d1* and NT*a3–d2* interactions were not significantly different, at 3.1 ± 0.4 and 3.9 ± 0.6 nM, respectively. Binding to GST was negligible, as were the signals obtained when either analyte or ligand protein were omitted (Fig. 1B).

LUTEOLIN INHIBITS THE NT*a3–d2* INTERACTION

Having modeled the *a3–d2* interaction using ELISA, we adapted this assay for high-throughput screening for small molecule inhibitors, as we have described previously [Kartner et al., 2010]. A pilot-scale screen was then executed with libraries of 1,120 marketed drugs (Prestwick Chemical), 1,280 pharmacologically active compounds (LOPAC^{1280}; Sigma) and 1,280 select bioactive compounds (Spectrum Collection; Microsource Discovery Systems), totaling 3,680 compounds. This yielded several primary hits for inhibition of the *a3–d2* interaction (hits being defined as having a B-score [Brideau et al., 2003] >3 SD below the mean). Rescreening of primary hits was done to determine dose response in the protein interaction assay, and toxicity in cellular assays. Only one compound, luteolin (Fig. 2A), a naturally occurring flavonoid, was found to be reproducibly and significantly inhibitory without overt cytotoxicity. The dose-response curves for inhibition of the *a3–d1* and *a3–d2* interactions by luteolin are shown in Figure 2B. They were not significantly different, with half-maximal concentrations for inhibition (IC_{50}) at 2.6 ± 0.9 μM for *a3–d1* and 2.4 ± 0.9 μM for *a3–d2*. Secondary screens were subsequently performed to determine dose-responses for the effects of luteolin on cell viability, osteoclast differentiation, and osteoclast resorptive activity.

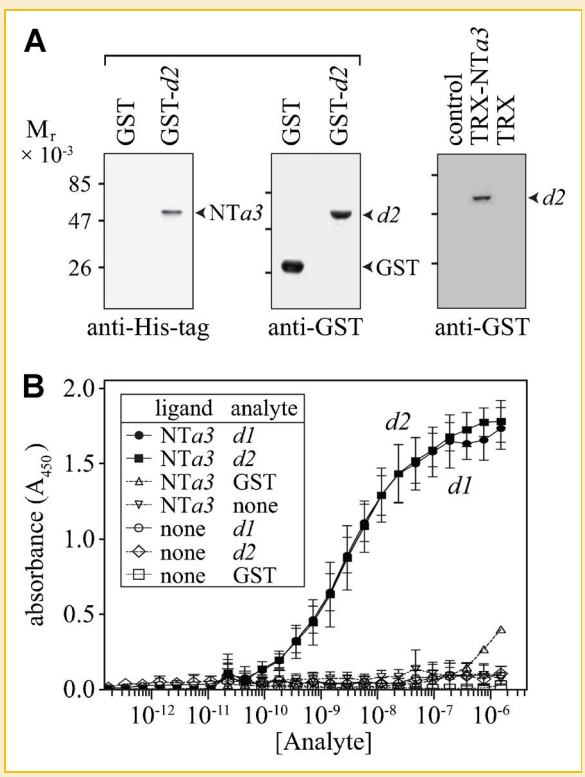

Fig. 1. NT*a3* interacts with *d1* and *d2* with identical apparent affinities. A: (Left and center panels), glutathione affinity beads were coated with GST-*d2* or GST alone, then incubated with TRX-NT*a3*. Protein was SDS-eluted from washed beads and immunoblotted with anti-His-tag or anti-GST antibodies (TRX contains a His-tag). Right panel: Ni(II) affinity beads were coated with TRX-NT*a3*, TRX alone, or were treated with buffer only (control), then incubated with GST-*d2*, processed like the glutathione beads and probed with anti-GST antibody. Note that blots are not in exact horizontal alignment with respect to molecular weights. B: ELISA saturation binding curves for NT*a3–d1* (●) and NT*a3–d2* (■) interactions. ELISA plates were coated with TRX-NT*a3* (ligand) and probed with GST-*d1* and GST-*d2* (analytes) from concentrations of 1.5 μM to 0.18 pM in a twofold dilution series. A_{450} indicates amount of analyte bound (see "Materials and Methods"). Negative controls were: NT*a3* ligand with GST analyte (△); NT*a3* ligand with no analyte (▽); no ligand with *d1* (○), *d2* (◇), or GST (□) analytes. Results are means; error bars are ±SD (n = 4, in quadruplicate).

LUTEOLIN IS NOT TOXIC TO NIH/3T3 AND RAW 264.7 CELLS

To assess the effect of luteolin on cell viability, the RAW 264.7 mouse macrophage cell line and the NIH/3T3 mouse fibroblast cell line were grown in the presence of a concentration range of luteolin for 3 days. Cells were subsequently tested in the mitochondrial

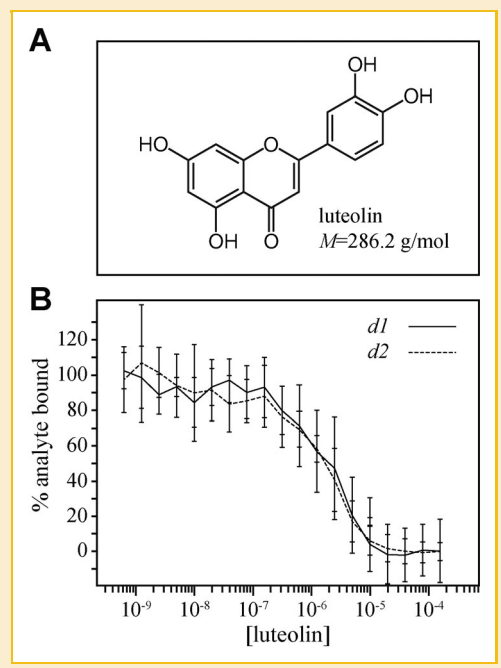

Fig. 2. Luteolin inhibits V-ATPase *a3–d2* interaction. A: Structure of luteolin, 3′,4′,5,7-tetrahydroxyflavone. B: ELISA-based binding assay, where TRX-NT*a3* ligand was probed with GST-*d1* or GST-*d2* analyte in the presence of luteolin (twofold serial dilution, 160 μM to 0.6 nM). A_{450} indicated amount of analyte bound (see "Materials and Methods"). A_{450} was normalized by background subtractions and conversion to percentages of controls without luteolin. Results are means; error bars are ±SD (n = 4, in quadruplicate).

reductase-based MTS assay to assess metabolic activity, and were assayed for total protein to assess growth. According to the MTS assay RAW 264.7 and NIH/3T3 cells were not significantly affected at any luteolin concentration used, suggesting that luteolin, at concentrations up to 40 μM, is not toxic to either cell line (Fig. 3A). Furthermore, under the same growth conditions, total protein content was unaffected at up to 40 μM luteolin (Fig. 3B). These data strongly suggest an $IC_{50} \gg 40$ μM for luteolin cytotoxicity in the proliferation assays employing either the RAW 264.7 or NIH/3T3 cell culture models.

LUTEOLIN DOES NOT AFFECT OSTEOCLASTOGENESIS OF RAW 264.7 AND BMM CELLS

We further investigated whether luteolin had any adverse effects on osteoclast differentiation and maturation by assaying TRAP. This early enzyme marker of osteoclastogenesis is readily detectable in mononuclear pre-osteoclasts, through to mature osteoclasts. Figure 4A,B shows the effect of luteolin on the number of TRAP-positive multi-nucleated osteoclasts differentiated from RAW 264.7 cells in the presence of recombinant RANKL, and BMM cells in the presence of recombinant RANKL and M-CSF, respectively. Histograms are shown normalized to untreated samples. The osteoclast counts were subdivided into three subpopulations: 2–5, 6–12, and ≥13 nuclei to determine the effect of luteolin on osteoclast size, which is a contributing factor for osteoclast resorptive activity [Manolson et al., 2003]. Osteoclast counts for RAW 264.7 and BMM cells appeared to decrease marginally up to 40 μM, but this was not statistically significant and all subpopulations were similarly affected.

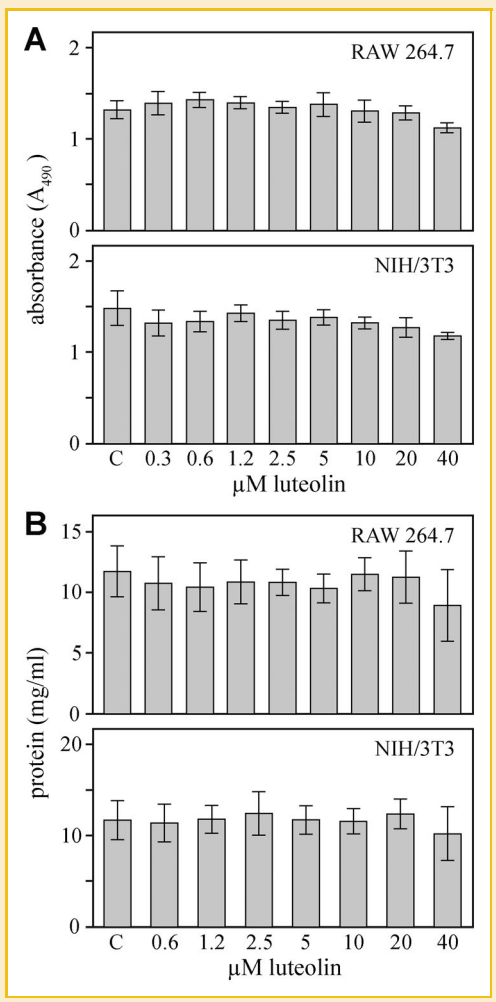

Fig. 3. Luteolin is not toxic to RAW 264.7 or NIH/3T3 cells. Cells were cultured in the presence of luteolin (twofold serial dilution, 40–0.3 μM). A: After 3 days continuous exposure, metabolic activity was assessed using MTS tetrazolium dye assay. Differences were not significant. B: Cellular protein was measured as an indicator of cell growth; untreated cells (C) were not exposed to luteolin. Differences were not significant. Results are means; error bars are ±SD (n = 3, six replicates each).

Figure 4C shows example images of BMM-derived osteoclasts, grown in the absence or presence of 5 μM luteolin on ivory (upper images) and Osteo Assay surface (lower images). Osteoclast morphology varied on these surfaces, having a rounded appearance on ivory and a flattened, fibroblastoid appearance on the synthetic hydroxylapatite of the Osteo Assay surface; however, the sizes of the osteoclasts did not significantly differ, whether untreated or treated with luteolin, on either surface. In RAW 264.7 cells the level of intracellular TRAP measured was not significantly different between treated and untreated samples, as shown in Figure 4D. The histogram is normalized to untreated samples and again suggests that, in the TRAP assay for differentiation, luteolin has an $IC_{50} \gg 40$ μM.

LUTEOLIN SUPPRESSES RESORPTIVE ACTIVITY IN RAW 264.7- AND BMM-DERIVED OSTEOCLASTS

To assess the efficacy of luteolin as a potential anti-resorptive agent, RAW 264.7 and BMM-derived osteoclasts were plated on a hydroxylapatite mineral surface (Corning Osteo Assay surface) and on dentin (elephant ivory) in the presence and absence of luteolin. The former medium is a recently introduced synthetic surface that lends itself to high-throughput screening, but it is just gaining acceptance as an assay for osteoclast resorption. The latter, on the other hand, is difficult to obtain and tedious to work with, but is regarded as a standard for osteoclast resorption assays, so we have included it by way of comparison. The thicker dentin also provides the only means of assessing resorption pit depths. For resorption on synthetic hydroxylapatite, both RAW 264.7 and BMM cells were plated directly on Osteo Assay plates and differentiated into osteoclasts for 5 days with exposure to 1.2–40 μM luteolin. Figure 5A shows photomicrographs of Osteo Assay surface partially resorbed by RAW 264.7-derived osteoclasts at various luteolin concentrations. Figure 5B shows quantification of the dose-dependent inhibition by luteolin of Osteo Assay surface resorption by osteoclasts derived from either RAW 264.7 or BMM cells, as indicated. Approximate EC_{50} values for luteolin inhibition of osteoclast resorption were 1.2 μM for RAW 264.7-derived cells and 2.5 μM for BMM-derived cells.

By direct observation, isolated resorption pits formed by BMM-derived osteoclasts on the Osteo Assay surface in the presence of luteolin appeared shorter than those of untreated controls. Thus, to assess more precisely how resorption pit morphology is affected by luteolin, we differentiated BMM cells on dentin and observed pits using Z-stacking confocal microscopy. An example of a resorption

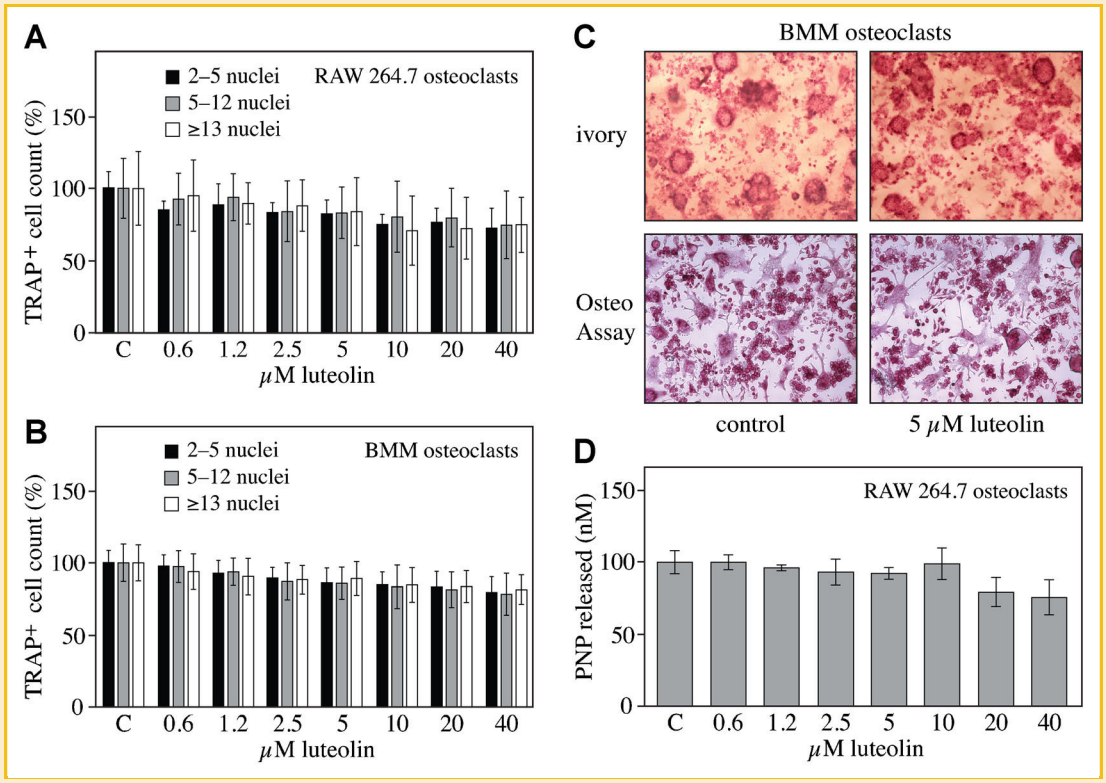

Fig. 4. Luteolin does not affect osteoclastogenesis in RANKL-induced RAW 264.7 and BMM cells. A: RAW 264.7- and (B) primary mouse BMM-derived osteoclasts, differentiated in the presence of 0.3–40 μM luteolin with RANKL, or with RANKL and M-CSF, respectively, for 5–7 days (see "Materials and Methods"). TRAP-stained, fixed cultures were counted for number of nuclei per cell in three cohorts: 2–5 (black), 5–12 (gray), and ≥13 (white) nuclei per cell. Results are means; error bars are ±SD (n = 3, in quadruplicate). C: (top row) TRAP-stained BMM osteoclasts differentiated without (control), or with 5 μM luteolin on ivory; (bottom row) TRAP-stained BMM osteoclasts differentiated without (control), or with 5 μM luteolin on Corning Osteo Assay surface. D: Total TRAP activity was assayed as *p*-nitrophenol (PNP) released by TRAP activity in solubilized RAW 264.7 cells, prepared as described in "Materials and Methods" and normalized to untreated (C) cells (n = 3, in triplicate).

pit and its 3D-rendered image is shown in Figure 5C. Pit lengths, areas, and depths were quantified and pit volumes were calculated. These data are represented graphically in the four panels of Figure 5D. We observed a highly significant decrease even at 0.6 μM, relative to controls, but no dose dependence across samples treated with 0.6–20 μM luteolin (Fig. 5D, upper left). Although luteolin decreased resorption pit depth overall compared to untreated controls, pit depth paradoxically increased with higher luteolin concentrations (Fig. 5D, upper right). Pit area, in contrast, followed an expected dose-dependent decrease with luteolin concentration (Fig. 5D, lower left). Because of the opposite slopes of the pit depths and pit areas in response to increasing luteolin concentration, the calculated pit volumes fall off sharply (by approximately 80%) at 0.6 μM luteolin, relative to control, but show no further significant decreases up to 20 μM luteolin.

LUTEOLIN DOES NOT INHIBIT ACTIN RING FORMATION

We asked next whether luteolin affects the ability of osteoclasts to form an osteoclast–bone interface. Actin rings are regarded as markers of osteoclast activation, remodeling their membranes to create sealing zones between the cell and bone during resorption [Feng et al., 2009]. BMM-differentiated osteoclasts were fixed and probed with the F-actin stain, phalloidin, to observe the effect of luteolin on actin ring formation (examples shown in Fig. 6A). Luteolin, up to 20 μM, did not have any observable effect on actin ring formation or sealing zone width (Fig. 6B). Downregulation of *a3* expression [Feng et al., 2009], or mutations of *a3* [Ochotny et al., 2011] have been shown, similarly, to have no effect on osteoclast actin rings.

LUTEOLIN HAS NO EFFECT ON V-ATPase SUBUNIT EXPRESSION, OR V-ATPase ASSEMBLY

To begin to address the molecular mechanism of luteolin action, we first investigated its effect on V-ATPase expression and assembly in osteoclasts. RAW 264.7 osteoclasts, differentiated for 5 days in the presence of 1.2, 10, and 20 μM luteolin were lysed and microsomal membranes were obtained by differential centrifugation. Immunoblots of microsomal membrane proteins were probed with antibodies specific to the V-ATPase V_0 subunits *a3* and *d2*, and the V_1 subunit E (Fig. 7A shows one example of three independently derived blots) and quantified with signals normalized to β-actin. These data (band intensities) were quantified as the ratios of *a3*/*d2* (V_0/V_0), *a3*/E (V_0/V_1), and *d2*/E (V_0/V_1), all normalized to β-actin (Fig. 7B). None of these ratios, across the range of luteolin concentrations, changed significantly relative to controls. These results indicate that the luteolin-dependent reduction of resorptive

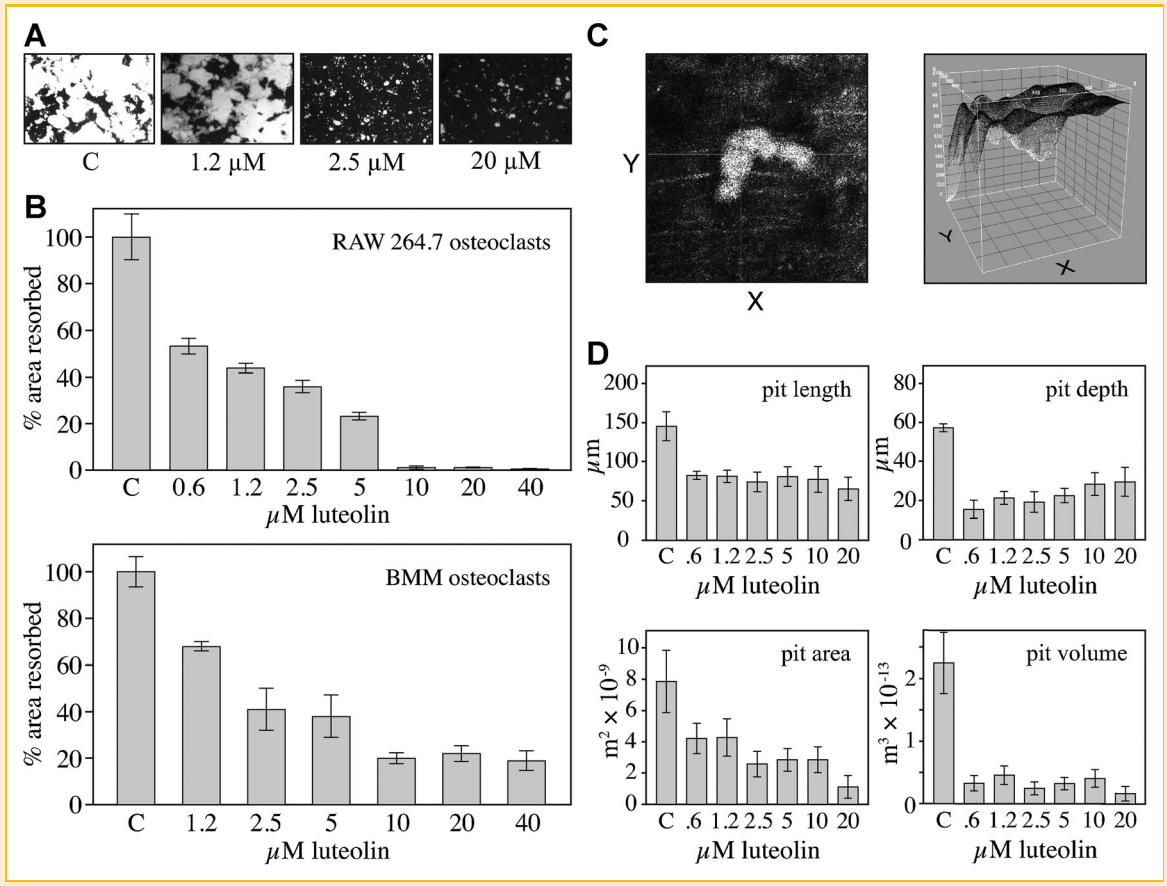

Fig. 5. Luteolin suppresses osteoclast resorptive activity. A: RAW 264.7 osteoclasts were grown on Corning Osteo Assay plates with luteolin for 5 days (C, without luteolin). Remaining mineral was von Kossa stained (black) and imaged, as described in "Experimental Procedures." Areas of resorption are white. B: Quantification of panel A experiments. Upper panel: RAW 264.7-derived osteoclasts on Osteo Assay plates without (C), or with 0.6–40 μM luteolin for 5 days. Lower panel: BMM-derived osteoclasts without (C), or with 1.2–40 μM luteolin for 5 days. Percent area resorbed (white area divided by total area) was quantified using NIH ImageJ after stripping cells and von Kossa staining plates for photomicrography. C: (left panel) shows a confocal image of a Picro-Sirius Red stained resorption pit in ivory, made by a BMM osteoclast. Right panel: 3D rendering (NIH ImageJ) of the confocal Z-stack of the pit in the left panel. D: BMM-derived osteoclasts on ivory without (C) or with 0.6–20 μM luteolin for 8 days. Cells were stripped and ivory slices stained with Picro-Sirius Red, as in panel C. Pit lengths, areas and depths were measured in confocal images using ImageJ and Volocity software. Pit volumes were estimated as the products of pit areas and pit depths × 0.5. All data from images are means normalized to untreated controls (C); error bars are ±SD (n = 3, in triplicates of five imaged fields per point).

activity is not due to an effect on osteoclast V-ATPase subunit expression or assembly.

DISCUSSION

CHARACTERIZATION OF THE *a3–d* INTERACTION

The V-ATPase complexes in the ruffled border are thought to contain specifically the *a3* and *d2* subunit isoforms that are highly enriched in osteoclasts. Furthermore, the *a3* and *d2* subunits are known to interact, as we and others have shown, and both are required for bone resorption [Toyomura et al., 2000; Manolson et al., 2003; Lee et al., 2006; Wu et al., 2009; Toei et al., 2010]. We hypothesized that small molecule inhibitors of the *a3–d2* interaction might have an impact on ruffled border V-ATPase function, resulting in reduced osteoclast bone resorption. To test this hypothesis we first set out to characterize the specificity and affinity of the *a3–d2* interaction.

Wu et al. [2009] previously compared interactions of *a3*, *d1*, and *d2* subunits and reported a "more extensive interaction" for *a3–d2*, compared with *a3–d1*. This observation was based on the ability of the recombinantly expressed, His-tagged *a3* subunit to co-immunoprecipitate more GST-*d2* than GST-*d1*. In contrast, using an ELISA-based solid-phase binding assay, we found that the *a3–d1* and *a3–d2* interactions were indistinguishable (Fig. 1B). This discrepancy likely reflects the limitation of comparing gel band intensities from co-immunoprecipitations to assess differences in binding affinities. Indeed, we found similar discrepancies in our own previous work when characterizing *a*-B subunit interactions [Kartner et al., 2010]. While solid-phase binding assays also have limitations with respect to determining true binding affinities, they have the advantage of being quantitative, and half-maximal binding values can be used to directly compare apparent affinities between subunit isoforms. Thus, based on saturation binding curves, we concluded that *a3–d1* and *a3–d2* interactions in V-ATPases are essentially identical.

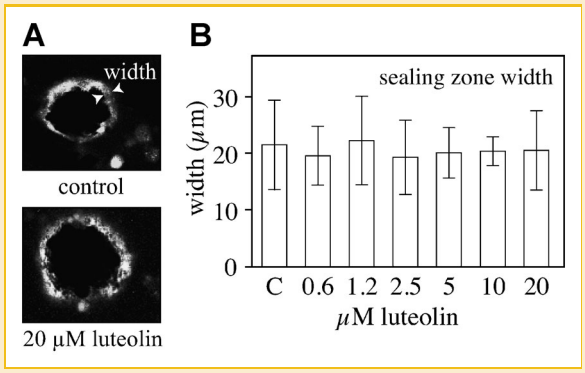

Fig. 6. Luteolin does not inhibit osteoclast actin ring formation. A: Phalloidin-stained actin rings of BMM osteoclasts; qualitatively, F-actin ring formation was not different, with or without luteolin. Ring width is indicated by arrowheads ("width," top panel). B: BMM cells were differentiated into osteoclasts without (C), or with 0.6–20 μM luteolin for 7 days on ivory (see "Experimental Procedures"). No significant differences in actin ring width were observed between untreated (C) and treated osteoclasts. Results are means; error bars are ±SD (n = 3, in duplicate).

HIGH THROUGHPUT SCREENING FOR INHIBITORS OF THE *a3–d2* INTERACTION

By adapting the above described solid-phase binding assay to a high-throughput screening format, we were able to perform a pilot-scale screen of natural and synthetic compounds for inhibitors of the *a3–d2* interaction. Small libraries of previously described compounds that are bioactive, or have a pre-clinical or clinical trial history, were chosen since any hits of interest could potentially be fast-tracked for FDA IND approval. This is a common first-run screening strategy for drug discovery by academic laboratories or small biotech companies. A promising hit that was identified in this screen was the natural product flavonoid, luteolin. Determining dose-response in the solid-phase binding assay revealed that luteolin had an IC_{50} for inhibition of the *a3–d2* interaction in the low micromolar range. This suggested that it might have therapeutic potential, and this notion was further reinforced by studies demonstrating its lack of toxicity in the effective concentration range, and its ability to inhibit osteoclast bone resorption with an EC_{50} of approximately 2.5 μM.

BIOLOGICAL SIGNIFICANCE OF *a–d* INTERACTION

The apparent affinities observed for *a3–d* interactions (half-maximal binding at 3–4 nM) were similar to those previously observed for *a3*–B interactions (2–3 nM) [Kartner et al., 2010]. These are relatively high apparent affinities, suggesting biological significance. In comparison, affinities obtained for B2–F-actin interaction ($K_d = 55$ nM) and *a2*–ARNO interaction ($K_d = 310$ nM) are approximately 20-fold and 100-fold lower, respectively, yet those interactions are known to be of biological importance [Lee et al., 1999; Merkulova et al., 2010].

What the biological significance of *a–d* subunit interactions might be remains largely speculative. Since the *a* subunit is part of the V-ATPase stator and the *d* subunit is part of the rotor, it seems likely that any *a–d* interaction must be transient in the functional

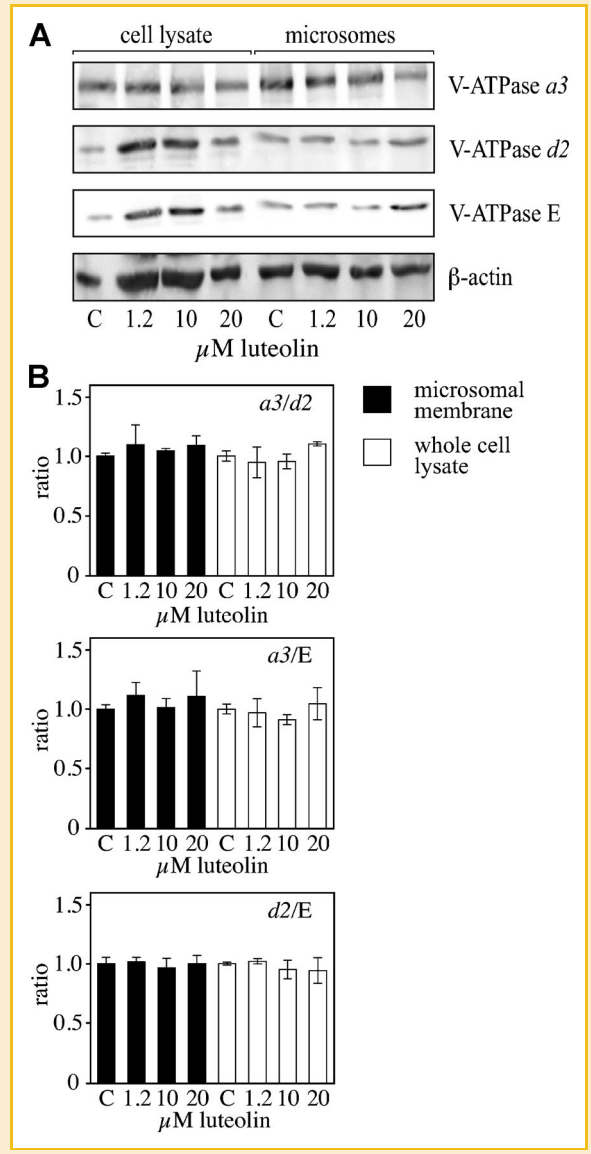

Fig. 7. Luteolin does not affect V-ATPase subunit protein expression or assembly. RAW 264.7 cells were differentiated into osteoclasts without (C), or with luteolin (1.2, 10, and 20 μM) for 5 days. Whole cell lysates and microsomal membranes were immunoblotted to assess V-ATPase assembly and subunit expression. A: Immunoblots of microsomal membranes and whole cell lysates probed with antibodies specific to V-ATPase V_0 subunits, *a3* and *d2*, and V_1 subunit E; anti-β-actin staining is a loading control. All bands shown are from the same blot (one of three blots used for quantification). B: Quantitative analysis of bands in panel A; ratios of *a3*/*d2* (top, both V_0 sector), *a3*/E (middle, V_0 sector vs. V_1 sector) and *d2*/E (bottom, V_0 sector vs. V_1 sector) were calculated. No significant differences (at $P < 0.05$) were observed between untreated (C) and treated osteoclasts. Results were normalized to β-actin; error bars are ±SD (n = 3).

complex. Alternatively, it could be argued that the interaction is important for accurate alignment of the V_1 and V_0 sectors during regulatory dissociation and reassociation of the V-ATPase complex, or that the NT*a* domain of the *a* subunit collapses onto the *d* subunit after V_1–V_0 dissociation to prevent reverse rotation of the rotor *c*-barrel from dissipating the established proton gradient. These

alternative scenarios seem unlikely, as we did not observe any effect of luteolin on V-ATPase dissociation, or assembly.

Single-particle electron microscopy has revealed that V-ATPases are closely related to F_1F_O-ATP synthases (F-ATPases). F-ATPases carry out sequential catalysis at three sites, radially separated by 120° around the rotor axis. Shimabukuro et al. [2003] showed that each step of F_1 rotor rotation is divided into two substeps, 80° for ATP binding, and 40° for ADP/phosphate release. In contrast, Yokoyama and co-workers have shown that, irrespective of ATP concentration, the V-ATPase rotor dwells at 120° intervals, or once per catalytic cycle, without substeps [Furuike et al., 2011]. It seems possible that *a–d* subunit interaction occurs during the "transient dwell time" of the proton translocation cycle. Moreover, it has been noted that for optimum function of V-ATPases, all the different subunits in the V_1 and V_0 sectors must be in correct alignment. We speculate that transient *a–d* interaction could serve to align the complex during the dwell time. Interference with this putative alignment mechanism possibly could impair the efficiency of rotation of the rotor complex, impacting the tightly coupled catalytic function of the V_1 sector.

DISCREPANCIES WITH EXISTING LITERATURE ON LUTEOLIN INHIBITION OF OSTEOCLAST FUNCTION

Luteolin has been previously characterized for its inhibitory effect upon osteoclasts [Zhang et al., 2008a; Lee et al., 2009] and its ability to decrease ovariectomy-induced bone loss [Kim et al., 2011] and titanium particle-induced osteolysis [Shin et al., 2012]. The results that we have presented here and those of the existing literature are in agreement with respect to the anti-resorptive properties of luteolin, yet there are significant differences in proposed mechanisms. We show that at low micromolar concentrations luteolin inhibits osteoclast resorptive activity without affecting osteoclast differentiation. In contrast, Lee et al. [2009], and the laboratory of Kim et al. [2011] and Shin et al. [2012], conclude that the anti-resorptive properties of luteolin are due to its inhibitory effect on osteoclast differentiation. The former study suggests that luteolin specifically inhibits the RANKL-induced signaling pathway in osteoclasts, and the latter works suggest that it also inhibits systemic pro-inflammatory cytokine release, but the proximal molecular target of luteolin was not identified.

There are numerous potential explanations for the differences within the existing literature and the present work. One variable is the source of luteolin. Zhang et al. [2008a] purified luteolin from the plant *Halenia corniculata*, while Lee et al. [2009], and the laboratory of Kim et al. [2011] and Shin et al. [2012], do not specify its source, and none of these authors address purity. Zhang et al. [2008a] and Kim et al. [2011], specify that DMSO was used as the carrier. It has been demonstrated that osteoclast differentiation is sensitive to low concentrations of DMSO [Lemieux et al., 2011], and it is possible that it might have synergistic effects with bioactive molecules, like luteolin. In the present work we used $\geq$98% pure luteolin (Sigma catalog no. L9283) in an aqueous stock solution. It is impossible, however, to assess objectively whether the solvent might contribute to variability of results, since insufficient details are given in the aforementioned cited works regarding controls and concentrations of DMSO present in experiments.

The difficulty in comparing the existing literature with our work is further compounded by the differences in methodology and source of osteoclasts (viz. vitamin D-induced co-cultures; or M-CSF and RANKL-induced bone marrow macrophages (at various concentrations of the cytokines); or RANKL and PD98059-induced RAW 264.7 cells). When direct comparisons are possible, substantial differences are seen within the published literature. For example, Lee et al. [2009] and Kim et al. [2011], report that when assaying differentiation of BMM-derived mouse osteoclasts, 1 μM luteolin results in 5% and 75% inhibition, respectively. In contrast, at 1 μM luteolin, we found no significant inhibition of differentiation. The differences with respect to BMM-derived osteoclasts most likely result from differences in culture conditions, and the timing of luteolin addition to the cultures. In the present work, BMM cells were first cultured for 2 days with M-CSF, prior to RANKL differentiation in the presence of luteolin. It has been previously noted that this 2-day pre-incubation period in M-CSF is essential for optimal osteoclast differentiation [Takahashi et al., 2003]. In contrast, Kim et al. [2011] include both RANKL and luteolin at Day 1 of culture. Furthermore, in their discussion, the authors note that addition of luteolin 1 day after the cultures were initiated did not significantly affect TRAP activity (data not shown), in agreement with our present results. More recently, Shin et al. [2012] showed reductions in numbers and size of osteoclast actin rings, with apparently reduced sealing zone widths at 10 μM luteolin concentration and nearly complete disorganization of actin rings at 20 μM concentration, without affecting cell viability. This was observed after differentiation of BMM cells in M-CSF and RANKL at one-fifth the concentration that was used in the present study, and in the presence of pro-inflammatory titanium nanoparticles, which are indirectly osteoclastogenic. These considerable differences in experimental conditions make it difficult to directly compare results, but they may account for the discrepancy with our own results, where actin rings were unaffected at the same luteolin concentrations.

With respect to the use of RAW 264.7 cells, Lee et al. differentiated RAW 264.7 cells in the presence of both 100 ng/ml RANKL and PD98059, an inhibitor of the MAP-kinases, MEK1, and MEK2 [Newton et al., 2000]; the addition of PD98059 was to enhance osteoclastogenesis. We do not use PD98059 and obtain comparable amounts of RAW 264.7-derived osteoclasts with 100 ng/ml RANKL alone. Although one might expect the presence of PD98059 to attenuate any inhibitory effect on osteoclastogenesis, MAP-kinases are involved in numerous other cellular processes, such as cell proliferation, motility, and apoptosis [Vojtek and Ders, 1998], and could possibly augment the effect of luteolin. As Kim et al. [2011] do not present any histological data with their ovariectomy-induced bone loss model, the ultimate question of whether luteolin protects against bone loss by inhibiting just osteoclast activity, or osteoclastogenesis, in vivo, remains unanswered. In the more recent work of Shin et al. [2012], which includes some histology, luteolin had a significant effect on titanium particle-induced recruitment of osteoclasts, but whether this is a special case, or luteolin more generally affects osteoclastogenesis, has yet to be established in vivo.

ANTI-RESORPTIVE POTENTIAL FOR TARGETING *a3–d2* INTERACTION AND MECHANISM OF ACTION

Although *a3* has the same apparent affinity for either *d1* or *d2*, and luteolin inhibits *a3–d1* and *a3–d2* interactions equally, lack of specificity may not be an issue affecting therapeutic targeting. There are differential expression patterns and functional differences between the two *d* isoforms. The amino acid identity between the two murine *d* isoforms is only 68%; this difference is reflected in the fact that in yeast, the murine *d1* can functionally complement yeast *d* ortholog (Vma6p) deletion, at 30°C, while *d2* could only partially complement at 25°C [Nishi et al., 2003]. While *d1* is ubiquitously expressed, *d2* expression is limited to bone, and at lower levels in kidney, heart, spleen, and testis [Nishi et al., 2003; Wu et al., 2009]. Within bone, *d2* is restricted to osteoclasts, where expression levels increase over 50-fold during differentiation [Wu et al., 2009]. Finally, while ablation of *d1* is embryonically lethal [Miura et al., 2003], knocking out *d2* in mice results in only a mild osteopetrotic phenotype [Lee et al., 2006]. The absence of *d2* in mice not only results in decreased osteoclast maturation and activity, but also increased osteoblast bone formation, an ideal outcome for an anti-resorptive therapeutic. In this regard, luteolin itself has been reported to stimulate osteoblast function [Choi, 2007].

We have demonstrated that luteolin inhibits the *a3–d2* interaction in a cell-free assay, and we have shown that osteoclast resorptive activity, which is V-ATPase dependent, is affected in a dose-dependent manner by luteolin. Nevertheless, we were unable to show that expression or assembly of V-ATPase subunits was affected. We have been unable to demonstrate effects of luteolin on V-ATPase catalytic activity, or proton translocation, because of the technical difficulties associated with performing such assays in the mammalian systems that were used in this report. Presently, the molecular mechanism of action of luteolin on V-ATPase remains uncharacterized. Thus, determining a precise mechanism of action will require further investigation and will be the focus of future work.

V-ATPase AS THE PROXIMAL TARGET FOR MULTIPLE EFFECTS OF LUTEOLIN

V-ATPase inhibition by luteolin may explain some of the other potentially therapeutic effects that have been reported for the compound, including its anti-cancer, anti-viral, and anti-inflammatory properties. Luteolin has been shown to decrease the viability and inhibit the invasive potential of the human breast cancer cell line MDA-MB231 [Attoub et al., 2011]. Hinton et al. [2009b] in their studies reveal that MDA-MB231 cells express higher levels of V-ATPase *a3* and *a4* isoforms. They also show that siRNA knockdown of either *a3* or *a4* significantly inhibits the invasiveness of MDA-MB231 cells. It is suggestive that the mechanism of luteolin as an anti-cancer agent that limits the invasive potential of MDA-MB231 breast cancer cells might be by targeting V-ATPase activity. Furthermore, many tumors are in poorly perfused compartments where their high metabolic activity results in significant local acidosis. To survive under such conditions they need to regulate cytoplasmic pH, and one of the key transporters required for this process is V-ATPase [Neri and Supuran, 2011]. Thus, luteolin may be more generally effective in limiting the viability of tumor cells by targeting V-ATPase activity.

Luteolin has also been previously shown to have the properties of an anti-viral agent preventing influenza virus infection [Liu et al., 2008]. V-ATPase-mediated lysosomal acidification is required for influenza virus infection, enabling the release of the virus from its receptor and translocation into the cytoplasm. V-ATPase-specific inhibitors have also been shown to inhibit replication/transcription of viral RNAs [Marjuki et al., 2011]. Thus, the proximal target of luteolin as an anti-viral agent may be the lysosomal V-ATPase. Similarly, luteolin has been characterized as having anti-inflammatory and other functions that typically involve activation or inhibition of various intracellular signaling pathways. Such outcomes can be affected by intracellular pH; therefore, it is worth considering in such cases that the proximal target of luteolin might be cellular V-ATPases, and that altered expression or activation of signaling molecules may be the secondary effects of altered intracellular pH.

OTHER CELLULAR EFFECTS OF LUTEOLIN

Osteolytic diseases create an imbalance between bone resorption and formation, and an ideal therapeutic would target osteoclast activity without affecting osteoclastogenesis [Tanaka et al., 2005; Walsh and Gravallese, 2010]. In our hands, luteolin did not affect RANKL-induced osteoclast differentiation and maturation. We examined the effect of luteolin on osteoclast genes: nuclear factor of activated T cells, cytoplasmic 1 (NFATc1), matrix metallopeptidase 9 (MMP9), and cathepsin K (CTSK), and found no significant difference between untreated and luteolin treated cells (at concentrations of 1.2, 10, and 20 μM; data not shown).

Typically, during bone resorption, osteoclasts pump protons onto the bone surface to dissolve microcrystalline hydroxylapatite and activate acid proteases to enzymatically degrade bone matrix proteins. Osteoclasts resorb bone to a certain depth and then move on, or undergo apoptosis. With time, there is an increase in number of resorption pits created by multiple osteoclasts, thereby leading to an increase in total resorbed surface. Our studies suggested that, in the presence of luteolin, osteoclasts continued to resorb bone; however, the size of their resorption pits was significantly diminished. In addition, there were fewer total resorptive events. Thus, luteolin not only decreased total resorption by osteoclasts, but also limited the depth of resorption pits by inhibiting the V-ATPase *a3–d2* interaction. There was, however a trend of increasing pit depth with increasing luteolin concentration. We postulate that reduction of pit area is due to reduction in osteoclast resorption activity, and the increase in pit depth at higher luteolin concentrations might be due to inhibition of osteoclast migration. In support of this notion, [Zhao et al., 2011] have shown that luteolin affects actin stress fiber formation, which is known to be involved in cell migration.

Immunoblots of osteoclast membrane revealed that V-ATPase subunits *a3*, *d2*, and *E* are synthesized normally and are not retained in the ER, or rapidly degraded. Thus, luteolin does not affect V-ATPase biosynthesis, assembly, or stability. Certain flavonoids have been previously shown to inhibit ATP synthesis and hydrolysis [Hong and Pedersen, 2008]; however, studies carried out by

Chinnam et al. [2010] show that inhibition by flavonoids is variable and that luteolin does not inhibit the ATPase activity of the homologous F_1F_O-ATP synthase. The precise mechanism of action of luteolin on V-ATPase activity therefore remains to be determined.

CONCLUSION

LUTEOLIN AS A POTENTIAL ANTI-RESORPTIVE THERAPEUTIC

In previous work, we characterized the interaction between V-ATPase *a3* and B2 subunits, which are enriched in osteoclasts, and then used an ELISA-based binding assay to screen small molecule libraries for inhibitors of the *a3*–B2 protein interaction [Kartner et al., 2010]. To assess whether this approach could be generally applied to osteoclast-specific subunit interactions we asked whether inhibitors of the known *a3–d2* interaction would yield similar results. Thus, we first expressed the *a3*, *d1*, and *d2* subunits as fusion proteins to investigate their binding characteristics. Using this information we then exploited our previously developed solid-phase binding assay approach to screen chemical libraries for inhibitors. Finally, we asked what the consequences are of inhibiting the *a3–d2* interaction in osteoclasts, with respect to cell viability, osteoclast differentiation and osteoclast resorptive activity.

In summary, here we have confirmed and further characterized the interaction between *a3* and *d* subunits of the mammalian V-ATPase, and showed that the naturally occurring flavonoid, luteolin, inhibits the *a3–d2* subunit interaction. Furthermore, we showed in cell culture experiments that treatment with micromolar luteolin concentrations resulted in reduced osteoclast bone resorption, without significantly affecting cell viability, morphology, or osteoclastogenesis. We conclude that the V-ATPase *a3–d2* interaction is a viable target for novel anti-resorptive therapeutics that potentially preserve osteoclast–osteoblast signaling important to bone remodeling. Considering this, it is possible that a specific inhibitor of the *a3–d2* interaction could therapeutically decrease bone resorption in bone-loss pathologies and, furthermore, that luteolin may serve as a lead candidate molecule for development of specific *a3–d2* inhibitors.

ACKNOWLEDGMENTS

We thank the following for their contributions to this work: Drs. Beth S. Lee and Brooke McMichael (Deptartment of Physiology and Cell Biology, Ohio State University College of Medicine, Columbus, OH) for providing cDNA clones for mouse *a3* subunits, anti-*a3*, and anti-E antibodies, and helpful discussions on Methods; Dr. Mario Filion (Alethia Biotherapeutics, Montreal, Canada) for his kind gift of anti-*d2* antibodies; Frederick Vizeacoumar and Thomas Sun (Samuel Lunenfeld Research Institute SMART robotics facility, Mt. Sinai Hospital, Toronto, Canada) for help with high-throughput screening; Feryal Sarraf and Nancy Valiquette (Faculty of Dentistry, University of Toronto, Toronto, Canada) for help with ivory sectioning and staining; Kirsten Krastel, Gursonika Binepal, Martha Cordova (Faculty of Dentistry, University of Toronto) for help with qRT-PCR and related discussions; Michael Woodside and Paul Partouis for advice and training in confocal microscopy; and the Toronto Zoo for the donation of elephant ivory. G.J.C. was supported by a scholarship from the Canadian Arthritis Society.

REFERENCES

Attoub S, Hassan AH, Vanhoecke B, Iratni R, Takahashi T, Gaben A-M, Bracke M, Awad S, John A, Kamalboor HA, Al Sultan MA, Arafat K, Gespach C, Petroianu G. 2011. Inhibition of cell survival, invasion, tumor growth and histone deacetylase activity by the dietary flavonoid luteolin in human epithelioid cancer cells. Eur J Pharmacol 651:18–25.

Brideau C, Gunter B, Pikounis B, Liaw A. 2003. Improved statistical methods for hit selection in high-throughput screening. J Biomol Screen 8:634–647.

Chinnam N, Dadi PK, Sabri SA, Ahmad M, Kabir MA, Ahmad Z. 2010. Dietary bioflavonoids inhibit *Escherichia coli* ATP synthase in a differential manner. Int J Biol Macromol 46:478–486.

Choi E-M. 2007. Modulatory effects of luteolin on osteoblastic function and inflammatory mediators in osteoblastic MC3T3-E1 cells. Cell Biol Int 31:870–877.

David Pe, Baron R. 1994. The catalytic cycle of the vacuolar H^+-ATPase. Comparison of proton transport in kidney- and osteoclast-derived vesicles. J Biol Chem 269:30158–30163.

Feng S, Deng L, Chen W, Shao J, Xu G, Li Y-P. 2009. Atp6v1c1 is an essential component of the osteoclast proton pump and in F-actin ring formation in osteoclasts. Biochem J 417:195–203.

Finnigan GC, Hanson-Smith V, Houser BD, Park HJ, Stevens TH. 2011. The reconstructed ancestral subunit a functions as both V-ATPase isoforms Vph1p and Stv1p in *Saccharomyces cerevisiae*. Mol Biol Cell 22:3176–3191.

Furuike S, Nakano M, Adachi K, Noji H, Kinoshita K, Yokoyama K. 2011. Resolving stepping rotation in Thermus thermophilus H^+-ATPase/synthase with an essentially drag-free probe. Nat Commun 2:1–9.

Henriksen K, Bollerslev J, Everts V, Karsdal MA. 2011. Osteoclast activity and subtypes as a function of physiology and pathology—Implications for future treatments of osteoporosis. Endocr Rev 32:31–63.

Hinton A, Bond S, Forgac M. 2009a. V-ATPase functions in normal and disease processes. Pfluegers Arch/Eur J Physiol 457:589–598.

Hinton A, Sennoune SR, Bond S, Fang M, Reuveni M, Sahagian GG, Jay D, Martinez-Zaguilan R, Forgac M. 2009b. Function of a subunit isoforms of the V-ATPase in pH homeostasis and in vitro invasion of MDA-MB231 human breast cancer cells. J Biol Chem 284:16400–16408.

Hong S, Pedersen PL. 2008. ATP synthase and the actions of inhibitors utilized to study its roles in human health, disease, and other scientific areas. Microbiol Mol Biol Rev 72:590–641.

Kandaswami C, Lee L-T, Lee P-PH, Hwang J-J, Ke F-C, Huang Y-T, Lee M-T. 2005. The antitumor activities of flavonoids. In Vivo 19:895–910.

Kartner N, Yao Y, Li K, Crasto GJ, Datti A, Manolson MF. 2010. Inhibition of osteoclast bone resorption by disrupting vacuolar H^+-ATPase *a3*–B2 subunit interaction. J Biol Chem 285:37476–37490.

Kawasaki-Nishi S, Bowers K, Nishi T, Forgac M, Stevens TH. 2001. The amino-terminal domain of the vacuolar proton-translocating ATPase a subunit controls targeting and *in vivo* dissociation, and the carboxyl-terminal domain affects coupling of proton transport and ATP hydrolysis. J Biol Chem 276:47411–47420.

Kim T, Ha H, Kim N, Park E-S, Rho J, Kim EC, Lorenzo J, Choi Y, Lee SH. 2010. ATP6v0d2 deficiency increases bone mass, but does not influence ovariectomy-induced bone loss. Biochem Biophys Res Commun 403:73–78.

Kim T-H, Jung JW, Ha BG, Hong JM, Park EK, Kim H-J, Kim S-Y. 2011. The effects of luteolin on osteoclast differentiation, function in vitro and ovariectomy-induced bone loss. J Nutr Biochem 22:8–15.

Lee BS, Holliday LS, Krits I, Gluck SL. 1999. Vacuolar H^+-ATPase activity and expression in mouse bone marrow cultures. J Bone Miner Res 14:2127–2136.

Lee S-H, Rho J, Jeong D, Sul J-Y, Kim T, Kim N, Kang J-S, Miyamoto T, Suda T, Lee S-K, Pignolo RJ, Koczon-Jaremko B, Lorenzo J, Choi Y. 2006. v-ATPase V_0 subunit d2-deficient mice exhibit impaired osteoclast fusion and increased bone formation. Nat Med 12:1403–1409.

Lee J-W, Ahn J-Y, Hasegawa S-i, Cha B-Y, Yonezawa T, Nagai K, Seo H-J, Jeon W-B, Woo J-T. 2009. Inhibitory effect of luteolin on osteoclast differentiation and function. Cytotechnology 61:125–134.

Lemieux JM, Wu G, Morgan JA, Kacena MA. 2011. DMSO regulates osteoclast development in vitro. In Vitro Cell Dev Biol Anim 47:260–267.

Liu A-L, Liu B, Qin H-L, Lee SM, Wang Y-T, Du G-H. 2008. Anti-influenza virus activities of flavonoids from the medicinal plant *Elsholtzia rugulosa*. Planta Med 74:847–851.

Manolson MF, Wu B, Proteau D, Taillon BE, Roberts BT, Hoyt MA, Jones EW. 1994. *STV1* gene encodes functional homologue of 95-kDa yeast vacuolar H^+-ATPase subunit Vph1p. J Biol Chem 269:14064–14074.

Manolson MF, Yu H, Chen W, Yao Y, Li K, Lees RL, Heersche JNM. 2003. The a3 isoform of the 100-kDa V-ATPase subunit is highly but differentially expressed in large ($\geq$10 nuclei) and small ($\leq$5 nuclei) osteoclasts. J Biol Chem 278:49271–49278.

Marjuki H, Gornitzky A, Marathe BM, Ilyushina NA, Aldridge JR, Desai G, Webby RJ, Webster RG. 2011. Influenza A virus-induced early activation of ERK and PI3K mediates V-ATPase-dependent intracellular pH change required for fusion. Cell Microbiol 13:587–601.

McMichael BK, Kotadiya P, Singh T, Holliday LS, Lee BS. 2006. Tropomyosin isoforms localize to distinct microfilament populations in osteoclasts. Bone 39:694–705.

Merkulova M, Bakulina A, Thaker YR, Grüber G, Marshansky V. 2010. Specific motifs of the V-ATPase a2-subunit isoform interact with catalytic and regulatory domains of ARNO. Biochim Biophys Acta 1797:1398–1409.

Miura GI, Froelick GJ, Marsh DJ, Stark KL, Palmiter RD. 2003. The d subunit of the vacuolar ATPase (*Atp6d*) is essential for embryonic development. Transgenic Res 12:131–133.

Neri D, Supuran CT. 2011. Interfering with pH regulation in tumours as a therapeutic strategy. Nat Rev Drug Discov 10:767–777.

Newton R, Cambridge L, Hart LA, Stevens DA, Lindsay MA, Barnes PJ. 2000. The MAP kinase inhibitors, PD098059, UO126 and SB203580, inhibit IL-1β-dependent PGE_2 release *via* mechanistically distinct process. Br J Pharmacol 130:1353–1361.

Niikura K. 2007. Effect of a V-ATPase inhibitor, FR202126, in syngeneic mouse model of experimental bone metastasis. Cancer Chemother Pharmacol 60:555–562.

Nishi T, Kawasaki-Nishi S, Forgac M. 2003. Expression and function of the mouse V-ATPase d subunit isoforms. J Biol Chem 278:46396–46402.

Ochotny N, Flenniken AM, Owen C, Voronov I, Zirngibl RA, Osborne LR, Henderson JE, Adamson SL, Rossant J, Manolson MF, Aubin JE. 2011. The V-ATPase a3 subunit mutation R740S is dominant negative and results in osteopetrosis in mice. J Bone Miner Res 26:1484–1493.

Pangrazio A, Caldana ME, Lo Iacono N, Mantero S, Vezzoni P, Villa A, Sobacchi C. 2012. Autosomal recessive osteopetrosis: Report of 41 novel mutations in the *TCIRG1* gene and diagnostic implications. Osteoporosis Int 271:3–8.

Scimeca J-C, Quincey D, Parrinello H, Romatet D, Grosgeorge J, Gaudray P, Philip N, Fischer A, Carle GF. 2003. Novel mutations in the *TCIRG1* gene encoding the a3 subunit of the vacuolar proton pump in patients affected by infantile malignant osteopetrosis. Hum Mutat 21:151–157.

Seelinger G, Merfort I, Schempp CM. 2008. Anti-oxidant, anti-inflammatory and anti-allergic activities of luteolin. Planta Med 74:1667–1677.

Shimabukuro K, Yasuda R, Muneyuki E, Hara KY, Kinosita K, Yoshida M. 2003. Catalysis and rotation of F_1 motor: Cleavage of ATP at the catalytic site occurs in 1 ms before 40° substep rotation. Proc Natl Acad Sci U S A 100: 14731–14736.

Shin D-K, Kim M-H, Lee S-H, Kim T-H, Kim S-Y. 2012. Inhibitory effects of luteolin on titanium particle-induced osteolysis in a mouse model. Acta Biomater 8:3524–3531.

Sobacchi C, Frattini A, Orchard P, Porras O, Tezcan I, Andolina M, Babul-Hirji R, Baric I, Canham N, Chitayat D, Dupuis-Girod S, Ellis I, Etzioni A, Fasth A, Fisher A, Gerritsen B, Gulino V, Horwitz E, Klamroth V, Lanino E, Mirolo M, Musio A, Matthijs G, Nonomaya S, Notarangelo LD, Ochs HD, Superti Furga A, Valiaho JA, van Hove JLK, Vihinen M, Vujic D, Vezzoni P, Villa A. 2001. The mutational spectrum of human malignant autosomal recessive osteopetrosis. Hum Mol Genet 10:1767–1773.

Takahashi N, Udagawa N, Tanaka S, Suda T. 2003. Generating murine osteoclasts from bone marrow. Methods Mol Med 80:129–144.

Tanaka Y, Nakayamada S, Okada Y. 2005. Osteoblasts and osteoclasts in bone remodeling and inflammation. Curr Drug Targets Inflamm Allergy 4:325–328.

Toei M, Saum R, Forgac M. 2010. Regulation and isoform function of the V-ATPases. Biochemistry 49:4715–4723.

Toyomura T, Oka T, Yamaguchi C, Wada Y, Futai M. 2000. Three subunit *a* isoforms of mouse vacuolar H^+-ATPase: Preferential expression of the *a3* isoform during osteoclast differentiation. J Biol Chem 275:8760–8765.

Vojtek AB, Ders CJ. 1998. Increasing complexity of the Ras signaling pathway. J Biol Chem 273:19925–19928.

Walsh NC, Gravallese EM. 2010. Bone remodeling in rheumatic disease: A question of balance. Immunol Rev 233:301–312.

Wu H, Xu G, Li Y-P. 2009. Atp6v0d2 is an essential component of the osteoclast-specific proton pump that mediates extracellular acidification in bone resorption. J Bone Miner Res 24:871–885.

Zhang J, Ahn M-J, Sun QS, Kim K-Y, Hwang YH, Ryu JM, Kim J. 2008a. Inhibitors of bone resorption from *Halenia corniculata*. Arch Pharm Res 31:850–855.

Zhang Z, Zheng Y, Mazon H, Milgrom E, Kitagawa N, Kish-Trier E, Heck AJR, Kane PM, Wilkens S. 2008b. Structure of the yeast vacuolar ATPase. J Biol Chem 283:35983–35995.

Zhao Y, Yang G, Ren D, Zhang X, Yin Q, Sun X. 2011. Luteolin suppresses growth and migration of human lung cancer cells. Mol Biol Rep 38:1115–1119.